Phase-Only Tuning of Extreme Huygens Metasurfaces Enabled by Optical Anisotropy

Ziwei Yang Mingkai Liu Andrei Komar Lei Xu Dragomir N. Neshev*

Ziwei Yang, Dr. Mingkai Liu, Dr. Andrei Komar, Dr. Lei Xu, Prof. Dragomir N. Neshev

ARC Centre of Excellence for Transformative Meta-Optical Systems (TMOS), Research School of Physics, The Australian National University, Canberra, ACT 2601, Australia

Email Address: dragomir.neshev@anu.edu.au

Keywords: *optical metasurfaces, liquid crystals, phase tunability*

Pure phase modulation of light is vital for a number of optical devices such as spatial light modulators and beam steering in light detection and ranging technologies. Tunable metasurfaces have recently provided a feasible alternative to existing technologies, allowing for ultra-high miniaturisation while enabling high transmission efficiency and tunability under small external stimuli. However, despite the recent advances in the field, no pure phase tuning has been demonstrated in transmissive devices, e.g. any implementation of continuous phase tuning is accompanied by sizable amplitude modulation or low efficiency. Here, we show that the optical anisotropy of the surrounding material can enable phase-only tuning of optical metasurfaces in the full 2π range with unitary efficiency over a sizable bandwidth. We further propose a practical implementation of this concept based on a liquid crystal infiltrated metasurface operating in the regime of extreme Huygens condition. In this way, we can enable the full 2π phase-only tunability in transmission by controlling bias voltage and temperature variation of the surrounding liquid crystal.

1 Introduction

Spatial light modulators (SLMs) are devices that can modulate light beam intensity and phase with two-dimensional spatial resolution [1]. An important class of such devices are the phase-only SLMs that transmit all of the incoming light with unitary power efficiency, while only modulating the transverse phase profile of the light beam. By encoding linear, parabolic or complex phase distributions, phase-only SLMs can be utilized as beam deflectors, lenses, and holograms, respectively. However, most devices to date exhibit large pixel size and low modulation phase, thereby preventing applications in efficient large-angle beam deflectors.

Over the last decade, optical metasurfaces [2] have emerged as a versatile platform for spatial light modulators, having sub-wavelength spatial resolution, highly miniaturized foot-print, and unique dispersive and polarization functionalities. Dielectric metasurfaces have further enabled unitary transmission efficiency [3–5], opening a plethora of applications for flat and smart optics. Important examples include applications such as flat lenses [6], axicons [7], and polarization holograms [5]. However, to date, most metasurfaces are static and cannot be dynamically reconfigured to enable variable phase modulation in the full 2π range that does not allow to use them as SLM devices.

Tunable metasurfaces have, thereby, been an area of intense research [8–10]. Various tuning approaches have been investigated, including carrier injection [11–14], temperature [15, 16], mechanical [17–19], and liquid crystals tuning [20–28]. However, all transmissive metasurfaces demonstrated to date cannot be tuned over a continuous full 2π-phase range or come at the expense of significant intensity modulation [14]. Therefore, new approaches to enable continuous 2π-phase tuning are required.

To realize such 2π phase-only tuning of optical metasurfaces, two major challenges remain to be resolved. Firstly, it is important to generate a sufficiently large phase change with a small external stimulus. Secondly, the transmission efficiency needs to be maintained close to unity during the tuning process. For example, in the case of tunable Huygens metasurfaces, which realize high transmission by the overlap of the electric and magnetic dipole resonances, the tuning process shifts the two resonances at a different rate. As a result the Huygens condition (and the unity transmission) is destroyed or can be maintained only in a narrow bandwidth [29]. In order to maintain the unity transmission, the tuning rates of the electric and magnetic resonances with respect to the external stimulus should ideally be identical. While there have been many attempts to hybridize tunable materials with Huygens metasurfaces, the

above two challenges have not been simultaneously addressed.

The integration of optical metasurfaces with liquid crystals (LCs) has proven a successful strategy to realize pronounced resonance tuning in metasurfaces. LCs are especially attractive for creating tunable metasurface devices, as they present a mature technology, which is extensively used for LC displays and thus offers clear perspectives for applications. Due to the LC anisotropy, the resonance positions can be dynamically controlled by the application of an external stimulus, such as temperature [20, 30] or voltage [21]. Based on that resonance tuning effect, several selected device functionalities, such as dynamic beam deflection [22, 31] and display action [32, 33] have been realized over the last few years. However, it remains elusive how to achieve a continuous phase-only tuning in transmission across a full 2π range. Importantly, there are no reports of such tuning using the conventional LC tuning mechanisms (temperature or voltage) alone. On the other hand, the ability to modulate the transmitted phase with unity efficiency is of utmost importance for advanced SLM applications including dynamic holography and lidar beam-steering. Thus, in order to allow for dynamic control of more complex metasurface functionalities, including freely programmable wavefront-shaping metasurfaces, it is important to develop novel concepts of pure-phase dynamic tunability with low external stimulus. However, pure-phase tunability in transmission has not been achieved to date at optical frequencies, and the physical mechanism for such a possibility remains to be explored.

Here, we propose a new method to realize 2π dynamic phase-only tuning in transmissive dielectric metasurfaces. We utilize the recent concept of *extreme Huygens metasurfaces* [34] that exhibit overlapping high-quality (high-Q) factor electric and magnetic resonances. The extreme-Huygens metasurface is immersed in a materials of tunable refractive index, which enables the tunability of the high-Q factor metasurface resonances by a weak change of this index. However, to tune both resonances at the same rate, a simple tuning of this refractive index in not sufficient. It is vital to explore the *optical anisotropy* of the surrounding material, which is critical to match the tuning rates of the electric and magnetic resonances. Based on this concept, we demonstrate a full 2π range tuning with a unity transmission by only changing the refractive index of the surrounding material by 2.5%. Such pure-phase modulation is achieved at telecommunication wavelengths with a sizable bandwidth of 31 nm. Finally, we propose a practical design based on a liquid crystal infiltrated extreme-Huygens metasurface tuned by manipulating the LC optical anisotropy using biased voltage and temperature.

2 Results and Discussion

2.1 Concept of optical anisotropic tuning

In our work we utilize a high-Q factor dielectric metasurface [34] immersed in a material with anisotropic refractive index, see Figure 1a. The operation principle of the extreme Huygens metasurface is based on our previous works on bound states in the continuum (BICs) metasurface, first introduced for optomechanical chirality [35] and then for bio-sensing [36]. The metasurface exhibits two strongly resonant modes with a Q-factor that is inversely proportional to the residual radiative loss. The high Q-factor is a result of minimising the mode overlap between the resonant modes and scattering channels. By tuning a structural parameter (in our case, the angle β as marked in Figure 1b), the overlap can be finely controlled. The Q-factor thereby will increase asymptotically, approaching infinity at $\beta \rightarrow 0$ [37]. While there have been a number of works exploring BICs states in metasurfaces over the past decade [38], the realization of a Huygens condition by overlapping two orthogonal BIC modes has largely remained unexplored. This extreme Huygens condition, however, shows a great future research and application potential [11, 34, 39].

Our extreme Huygens metasurface is a periodic array of units, consisting of four elliptical cylinders in a zig-zag arrangement, see Figure 1a-c. By rotating the elliptical cylinders, we can reduce the structural symmetry, allowing the originally dark modes (BICs) to become leaky states, also called quasi-BICs (QBICs). A unique property of this zig-zag design is that it can support two QBICs that have different mode symmetries along the vertical z-direction. As our previous study showed [34], the even mode is dominated by an electric dipole moment and the odd mode is dominated by a magnetic dipole moment (Figure 1b). Therefore, we dubbed these two modes electric and magnetic QBICs [34]. Importantly, since the linewidths of the electric-QBIC (E-QBIC) and the magnetic QBIC (M-QBIC) follow the same scaling rule with the angle β, their Q-factors can be adjusted with β over orders of magnitude in exactly the same way [34]. For conventional all-dielectric Huygens metasurfaces, the spectral linewidths of the electric and magnetic dipole resources are relatively broad, resulting in Q-factors of the order of 10. These broad spectral linewidths make it impossible to dynamically tune the resonance over its full width, to acquire transmissive phase tuning up to 2π even with a refractive index change as large as 0.2. On the other hand, extreme Huygens metasurfaces are based on QBICs modes, enabling experimental Q-factors of 100s and higher. Thereby they provide a practical pathway to narrowing the linewidth of the Huygens state, allowing for extremely dispersive pure phase modulation in transmission and dynamical 2π phase tuning

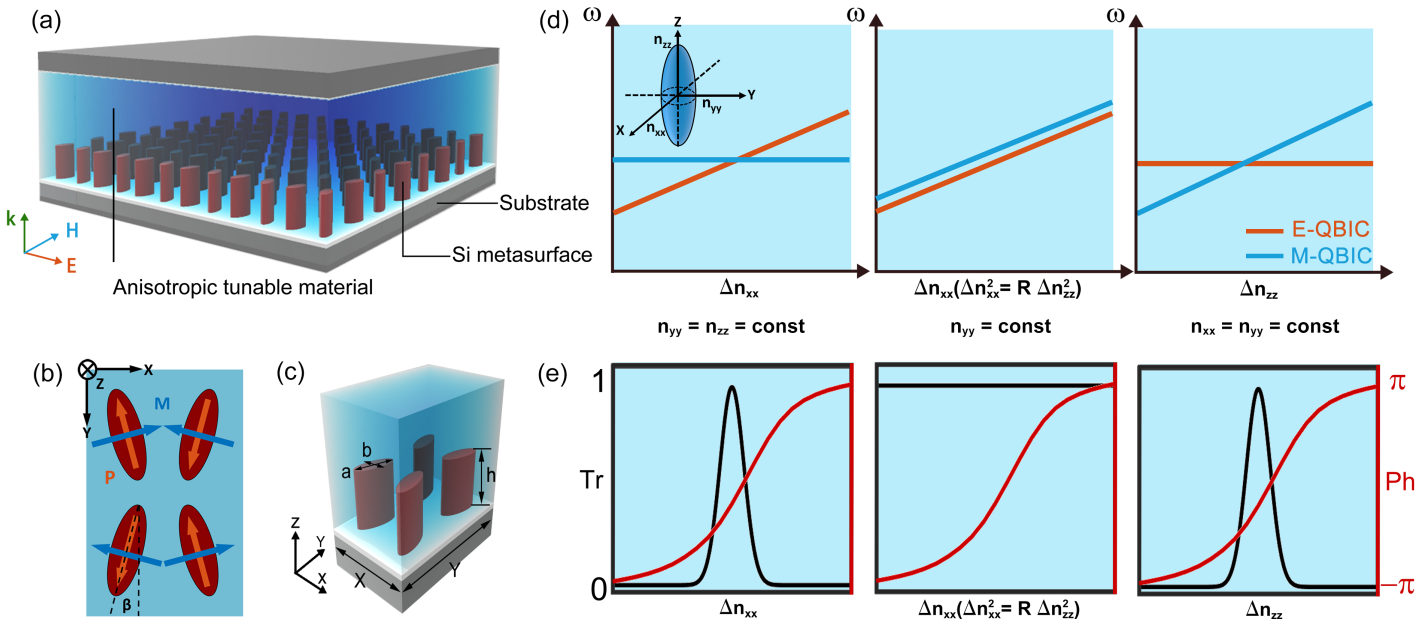

Figure 1: Tunable extreme-Huygens metasurface with optical anisotropy. (a) Schematics of a zig-zag extreme-Huygens metasurface infiltrated with an anisotropic tunable material. (b) Unit cell of the zig-zag metasurface (top view) exhibiting electric and magnetic quasi-bound-states in the continuum (QBICs) resonances. P and M are the corresponding electric and magnetic polarizations. (c) 3D view of the metasurface unit-cell infiltrated with an anisotropic material. X, Y are the periodicity along x and y direction, respectively; a, b are the major and minor axes of the elliptical cylinder, h is its height and β is the rotation angle. (d) Schematic diagrams of the tunability of the electric and magnetic resonances as a function of the different refractive index components of the refractive index ellipsoid, shown as an inset on the top left. The first and third plots show cases for a change in only one refractive index component, while the second plot changes two refractive index components simultaneously with a ratio of $\sqrt{R}$. By controlling the values of the refractive index tensor, it is possible to manipulate and synchronize the tuning rates of the electric and magnetic QBICs. (e) Transmittance (black line) and phase (red line) plots corresponding to (d) at a fixed wavelength.

with a much smaller external stimulus, e.g. refractive index change.

In this study, we consider elliptical cylinders made of hydrogenated amorphous silicon (a-Si:H) on a high-refractive index glass substrate (e.g. N-BAF10 glass with $n \approx 1.65$). The absorption of the a-Si:H at the operating wavelength of 1550 nm is negligibly small, allowing the transmittance to be above 0.95. Figure 1d shows the spectral positions of the two supported QBICs on a high transmission background (see also Figure S1 of the Supporting Information). The high refractive index difference between a-Si:H ($n \approx 3.52$) and the substrate ($n \approx 1.65$) produces resonances with strong field enhancement. Importantly, 81% and 59% of the electric fields of the E-QBIC and M-QBIC modes, respectively are distributed outside the silicon resonators, offering the metasurface an extensive sensitivity to changes of the surrounding environment.

An important requirement for establishing the Huygens condition is the orthogonality of the E-QBIC and the M-QBIC. The orthogonality of the two modes prevents their coupling and allows them to coexist at the same frequency. Since the presence of the substrate breaks the symmetry along the z-direction,

the refractive indices of the substrate and the surrounding anisotropic material have to be judiciously chosen to prevent the occurrence of mode coupling, hence anti-crossing. Alternatively, the metasurface needs to be encapsulated in the surrounding material to ensure symmetric environment and zero bi-anisotropy [40]. Both of these geometries are studied below.

To understand the underlying mechanism of metasurface tuning in optical anisotropic environment, first we study a dielectric metasurface immersed in a tunable birefringent material, as shown in Figure 1a,c. We describe how the resonances of the metasurface shift in response to the change of the different refractive index components of anisotropic environment. For simplicity, we assume that the orientation of the anisotropic environment is such that the refractive index tensor has only diagonal components,

$$\hat{n} = \begin{bmatrix} n_{xx} & 0 & 0 \\ 0 & n_{yy} & 0 \\ 0 & 0 & n_{zz} \end{bmatrix}. \tag{1}$$

Compared with other tuning mechanisms, such as carrier injection [11–13], temperature [15, 16], and mechanical tuning [17, 18], the simultaneous tuning of the different components of the anisotropic refractive index tensor offers a unique mechanism to match the tuning rates of electric and magnetic QBICs. Equalising the tuning rates of both resonances is crucial in maintaining the Huygens condition during the dynamic tuning and operating over a sizable bandwidth, exceeding the spectral width of each of the resonances.

We find that the tuning rate of resonance is primarily determined by the product of the dominant field components and the corresponding refractive index tensor components. Figure 1d,e illustrate the general concept of maximising and simultaneously equalising the tuning rates of different resonances by changing the anisotropic refractive index. When only one component of the refractive index tensor is changed, e.g. n_{xx} or n_{zz} in the left and right plots, correspondingly, only one of the resonances is significantly affected. Following the symmetry of the QBIC modes (see Figure S2 of the Supporting Information) the E-QBIC is affected by the change of n_{xx}, as the x-component of the electric field is dominant outside of the silicon elliptical cylinders. On the other hand, for M-QBIC the fields are predominantly along the z-direction, therefore this mode is mostly altered by the change of n_{zz}. These different tuning rates result in the Huygens condition being satisfied for only one frequency and refractive index (Figure 1d – left and right plots) and correspondingly leads to a strong change of the transmission with the tuning

of the individual refractive index components (Figure 1e – left and right plots). However, if both refractive indices (n_{xx} and n_{zz}) are tuned simultaneously, both tuning rates can be maximised and simultaneously equalised (Figure 1d – middle plot). It turns out there exists a 'magic ratio' between the change of the two refractive indices, $n_{xx} = \sqrt{R}n_{zz}$ with which the speed and direction of the shifts for both resonances are synchronized. In this regime, the Huygens condition is achieved for a broad range of wavelengths and tuning conditions. This type of anisotropic tuning also assures that the transmission phase can be tuned in the full range of 2π, while maintaining a unity transmission (Figure 1e – middle plot). Therefore, combining the anisotropic tuning concept with extreme Huygens condition provides the physical foundation to overcome simultaneously the two major challenges in SLM development, namely pure-phase tuning together with the use of small external stimuli for high-transmission metadevices.

To explain the working principle, we refer to the theoretical description of resonant eigenstates of periodic nano-resonators [41]. In this description, the electric field of an eigenmode is altered by a change of the refractive index, where the electric field of the modified eigenmode is proportional to the overlap integral,

$$V_{m,\mu} = \int_{\mathcal{V}} dV \mathbf{E}_m(\mathbf{r}; -\mathbf{k}) \cdot \Delta\hat{n}^2(\mathbf{r}) \mathbf{E}_\mu(\mathbf{r}; \mathbf{k}). \tag{2}$$

Here, $\mathbf{E}_m$ and $\mathbf{E}_\mu$ denote the electric field of the initial and modified eigenmodes at frequencies ω_m and ω_μ, respectively; $\mathbf{k}$ denotes the in-plane wave vector.

The relationship between the resonance shift and the refractive index change can then be described using the first-order perturbation theory when the refractive index change is small,

$$\Delta\omega \equiv \omega_\mu - \omega_m \approx -\frac{\omega_m}{2} V_{m,m}. \tag{3}$$

Equations 2 and 3 provide an important insight that the change of resonant frequencies depends not only on the spatial overlap of the refractive index change and the eigenmodes but also on the vectorial products of the refractive index tensor and the electric field vectors of the eigenmodes. If the refractive index change is isotropic, the resonant frequency shifts for the electric and magnetic QBICs are different. In this case, the two modes have different electric field profiles, hence their overlap integral $V_{m,m}$ with the scalar refractive index change $\Delta n(\mathbf{r})$ will be different. However, if the refractive index change is anisotropic, it is possible to utilize a new degree of freedom based on the vectorial nature of the eigenfields and the refractive index tensor, thereby to tailor the overlap integrals and thus the resonance shifts

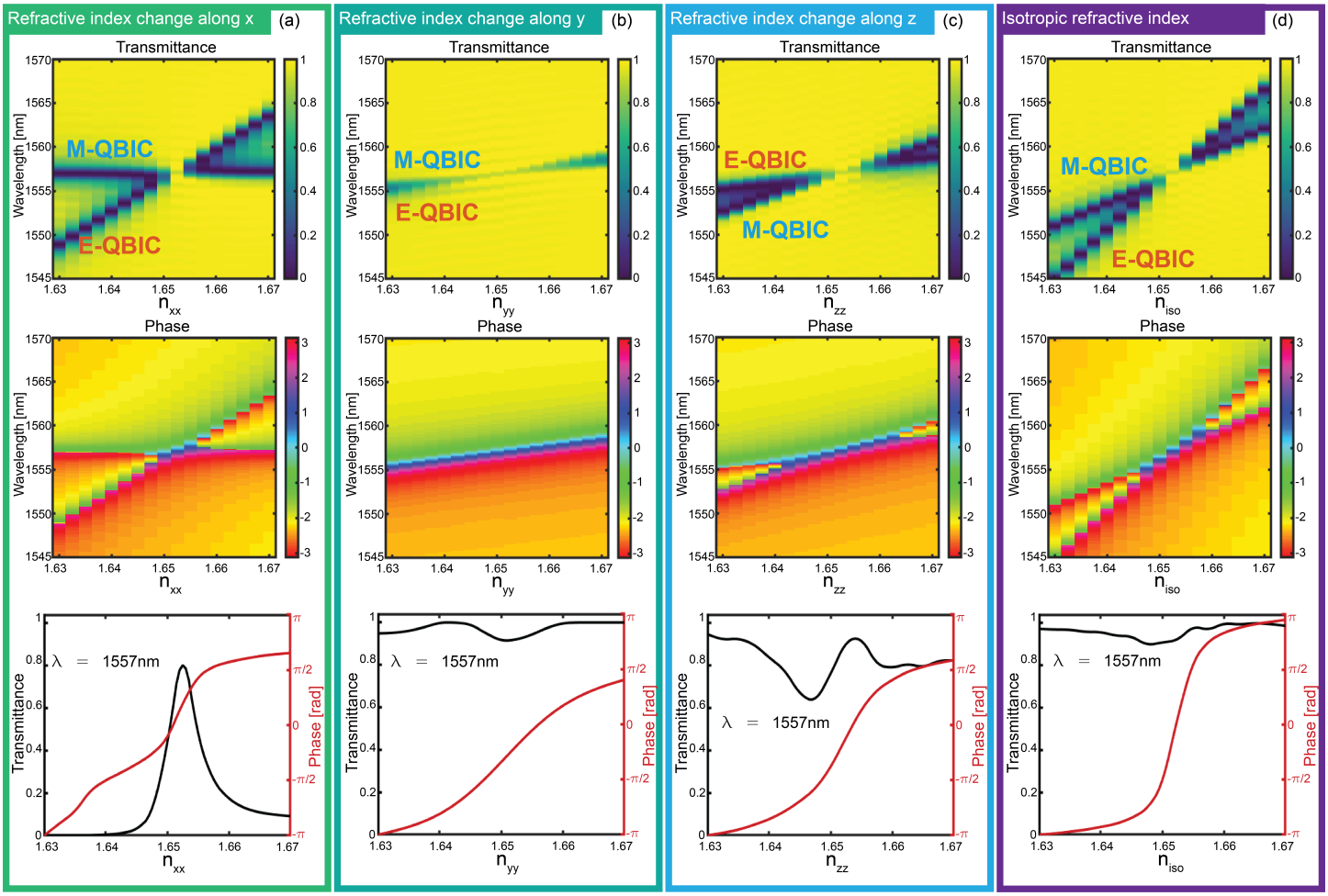

Figure 2: Resonance tuning of a zig-zag metasurface surrounded by an anisotropic material (no substrate). (a-d) Simulated two-dimensional transmittance and phase spectrum of the metasurface *vs* the refractive index change of the surrounding material. (a) Spectra when tuning n_{xx} from 1.63 to 1.67 while $n_{yy} = n_{zz} = 1.6525$; (b) Spectra when tuning n_{yy} ($n_{xx} = n_{zz} = 1.6525$); (c) Spectra when tuning n_{zz} ($n_{xx} = n_{yy} = 1.6525$); (d) Spectra when tuning all three components simultaneously $n_{xx} = n_{yy} = n_{zz} = 1.63 - 1.67$. The design parameters of the metasurface are: $X = 900$ nm, $Y = 1265$ nm, $a = 240$ nm, $b = 80$ nm, $h = 520$ nm. The rotation angle of the elliptical cylinder is $\beta = 8°$. Top row – simulated 2D transmittance spectra; middle row – 2D phase profile; bottom row – transmittance and phase of the metasurface at a wavelength of 1557 nm *vs.* the refractive index of the surrounding material.

of electric and magnetic QBICs.

To illustrate the potential of optical anisotropy, we simulate the resonance shifts of E-QBIC and M-QBIC using finite difference time domain (FDTD) method (Lumerical). In our simulations we use a unit cell with periodic boundary conditions along the x- and y-directions. The metasurface is excited with a plane wave polarised along the x-direction and propagating at normal incidence. We start with the simple example where the silicon resonators are fully surrounded by the anisotropic material, e.g. no substrate, no bi-anisotropy. Figure 2 shows the metasurface tuning as a result of the change of the different refractive index tensor components.

First, we simulate the transmission spectra when only changing a single component of the refractive in-

dex tensor. Figure 2a shows the result when n_{xx} is varied from 1.63 to 1.67, while n_{yy} and n_{zz} remain constant at 1.6525. In this case, the tuning rate of the E-QBIC is much higher than that of the M-QBIC. As mentioned before these different tuning rates are a result of the different vectorial components of the electric field and their overlap with the anisotropic refractive index tensor. The different tuning rates result in a Huygens regime only in a narrow range, where the transmittance is high (top plot). The overlap region is clearly seen in the phase profile (middle plot) but it results in a rapidly changing transmission and incomplete phase coverage at a fixed wavelength (bottom plot in Figure 2a).

When only the n_{yy} component is varied (Figure 2b), the two resonances red-shift with a similar tuning rate, however, both E-QBIC and M-QBIC demonstrate much weaker tuning. As a result, the wavelength range of the Huygens condition remains narrow, and incomplete phase coverage can only be achieved (see bottom plot). When increasing only the n_{zz} component and maintaining $n_{xx} = n_{yy} = 1.6525$, the M-QBIC shows a stronger shift as compared to E-QBIC (Figure 2c). Again, the Huygens condition is only satisfied at a narrow wavelength range, and the maximum phase shits is only around $3\pi/2$ (bottom plot), while the transmission decreases rapidly down to 0.6.

The main reason for the observed different behavior is that the mode fields of E-QBIC and M-QBIC have different dominant components in the surrounding environment. For example, the electric field generated by the E-QBIC is dominated by the x-component in environment, while the z-component of the electric field plays a significant role in the M-QBIC. The y-component, in contrast, primarily distributes inside the silicon part of the metasurface. This qualitatively explains why the E-QBIC responses stronger to the change in n_{xx} while the M-QBIC has a more noticeable shift with respect to the change of n_{zz}.

Finally, when the surrounding material is isotropic ($n_{xx} = n_{yy} = n_{zz} = n_{iso}$), the two Q-BICs generally show different rates of resonance shift. As such, the simultaneous increase of the three refractive index components, as in the case of an isotropic media, would result in a stronger tuning response. Figure 2d shows the transmittance and phase through the metasurface, simulated as a function of the surrounding isotropic refractive index. While the overall tuning rates in the isotropic case are indeed higher, it can be seen that the sensitivity of the electric resonance is larger than that of the magnetic resonance. As a result, the Huygens condition can be maintained only for a narrow spectral range, as seen in the plot of Figure 2d. We define the spectral bandwidth of operation as the region where the phase shift is larger than 1.75π while the transmission is higher than 50% (3 dB). The phase range $> 1.75\pi$ allows for 8 levels of discretization of the full 2π phase change that is enough for most practical applications.

Below we will refer to this range as 2π phase range. The spectral bandwidth in Figure 2d is then calculated to be 1.7 nm, which is similar to the spectral width of the individual resonances. We note that the full-width at half maximum (FWHM) of the E-QBIC or M-QBIC is 1.6 nm, resulting in a Q factor of around 980, see Figure S1 of the Supporting Information. Such narrow bandwidth unfortunately limits the applicability of isotropic surrounding materials for the phase-tuning of metasurfaces. The tuning rates of the two resonances in the four cases presented in Figure 2 are summarized in Table 1, we can clearly see that the shifting rate in the isotropic case is the superposition of the three tuning rates from the anisotropic cases.

	shifting rate $\Delta\omega/\Delta(n^2)$			
	n_{xx}	n_{yy}	n_{zz}	n_{iso}
E-QBIC	110.60	24.24	28.03	162.88
M-QBIC	2.27	21.97	59.85	83.33

Table 1: The calculated tuning rates of electric resonance and magnetic resonance when varying the corresponding refractive index tensor components.

It is important to note that while the isotropic case offers an opportunity for single wavelength phase modulation, the required refractive index change of ~ 0.04 is not feasible with conventional tuning mechanisms of common liquids. As an example, the thermo-optic tuning of liquids is of the order of $\Delta n \sim 10^{-3}$ [42], which is more than an order of magnitude weaker. By using anisotropic surrounding medium, we can overcome this limitation and accomplish two important results. On the fundamental side, we can equalise the tuning rates of both resonances thereby achieve Huygens tuning regime over a sizable spectral bandwidth. Such an achievement can have important implications for broadband or short-pulse type SLMs. On the practical side, the feasibility of the anisotropic tuning can be accomplished using liquid crystal type materials that offer refractive index change on the order of $\Delta n \sim 0.2$. Below we address these two points in detail.

First, we demonstrate the opportunity to equalise the tuning rates of both resonances. For this purpose, we tune two of the refractive index tensor components, namely n_{xx} and n_{zz}, at different rates. Surprisingly, with numerical simulations guided by the insight from Equation 2, we found that there exists a magic relation between the two tuning rates, where $\Delta n_{zz}^2 = R\,\Delta n_{xx}^2$, with $R = 2.78$. For this 'magic ratio', the two resonances red-shift at the same rate and an ideal broadband extreme Huygens regime is achieved. This regime is illustrated in Figure 3a-d. Due to the exact overlap of the E-QBIC and M-QBIC over the entire tuning range, the transmission through the metasurface is close to unity (Figure 3a) for a bandwidth of over 31 nm (Figure S4 of the Supporting Information). Such a bandwidth corresponds

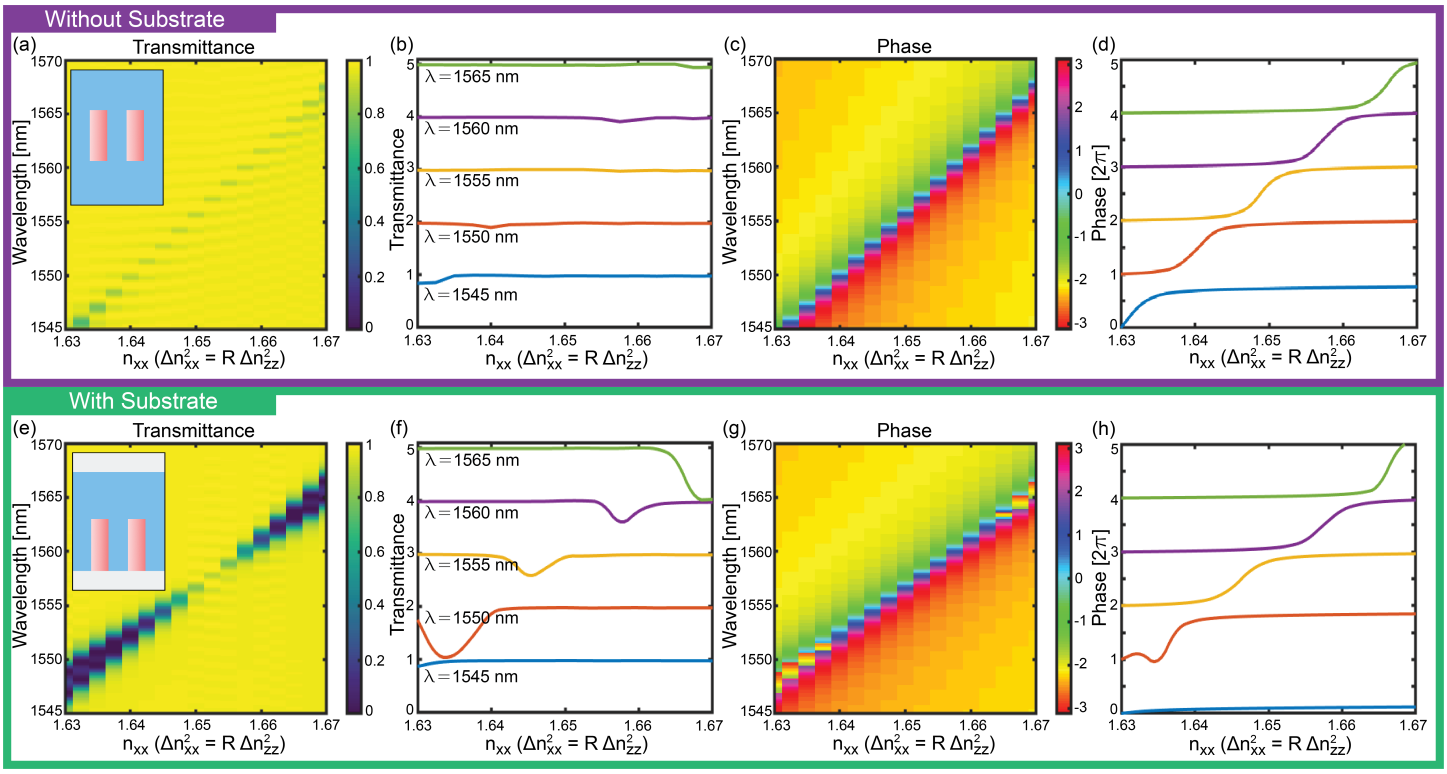

Figure 3: Broadband tuning of zig-zag extreme Huygens metasurfaces in symmetric environment (top) and with a substrate (bottom). (a) Simulated two-dimensional transmittance of the metasurface *vs* the refractive index components, n_{xx} and n_{zz}. The rates of change are proportional to each other: $\Delta n_{zz}^2 = R\,\Delta n_{xx}^2$, where $R = 2.78$. (b) Transmittance at five different wavelengths within the 31 nm bandwidth. (c) The calculated transmission phase spectrum, demonstrating perfect phase-only tuning over a broad bandwidth. (d) The transmitted phase for the five wavelengths corresponding to (b). (e-h) Corresponding transmittance and phase spectra of the metasurface placed on a high-index-glass substrate.

to operation with transform-limited femtosecond pulses with a pulse duration of 81 fs at the central wavelength of 1550 nm. The high transmission is easier seen with transmission plots at five different wavelengths presented in Figure 3b. Importantly, the phase profiles shown in Figure 3c,d cover the entire 2π phase range, enabling broadband SLM operation.

While such broadband operation is an impressive result, in practice the metasurface has to be positioned on a substrate for mechanical support. The substrate, however, introduces vertical (along the z-axis) bi-anisotropy, which breaks the degeneracy of the E-QBIC and M-QBIC and correspondingly disturbs the Huygens condition. The case of a metasurface placed on a high-index substrate ($n = 1.6525$) is shown in Figure 3e-h. Due to the presence of the substrate, the transmittance spectrum now shows a drop in transmission away from the central point of the Huygens regime, Figure 3e,f. Correspondingly, the spectral bandwidth of the tuning is reduced to 5.3 nm, which is still significantly higher than in the case of isotropic material (Figure 2d) and sufficient for operation with 480 fs pulses or longer. The 2π phase range is also preserved over this bandwidth (Figure 3g,h). Importantly, this bandwidth is three times the bandwidth of the individual resonances. Furthermore, such substrate-induced bi-anisotropy can be

removed by considering Huygens condition in suspended membrane-type metasurfaces [43].

2.2 Liquid crystal tunable extreme Huygens metasurface

To extend the results of our previous section to more realistic implementation, we consider liquid crystals (LCs) as the surrounding material for tuning the properties of our extreme Huygens metasurface. LC tuning is a promising approach to achieve pure phase tuning because of its large optical birefringence that can be controlled by electric field and temperature [44, 45]. For example, the refractive index of a popular LC mixture in display technologies, E7, can be tuned in the range $1.5 - 1.7$ for linearly polarized light [46]. It has already been shown that by using LCs, it is possible to control the response of metasurfaces by applying voltage to an LC cell where one of the substrates is a metasurface [21], by controlling the temperature of the cell [20] or both [47]. These works also demonstrated that the alignment of the LC molecules on top of the nanostructures happens even without an alignment layer, only by utilising the alignment layer on the top substrate of the LC cell.

Here, we combine two LC tuning mechanisms together, i.e. voltage and temperature, to maximize the phase tuning of our extreme Huygens metasurface. This is possible because for nematic uni-axial LCs, the ordinary and extraordinary components of the refractive index change differently with temperature. The temperature dependence is described by the equations,

$$\begin{aligned} n_o(T) &\approx A - BT - \frac{(\Delta n)_0}{3}\left(1 - \frac{T}{T_c}\right)^{\beta}, \\ n_e(T) &\approx A - BT + \frac{2(\Delta n)_0}{3}\left(1 - \frac{T}{T_c}\right)^{\beta}, \\ \langle n \rangle &= A - BT, \end{aligned} \tag{4}$$

where n_o and n_e are the ordinary and extraordinary component of the LC refractive indices, $\langle n \rangle$ is the average refractive index. In Equation 4, $(\Delta n)_0 = 0.3485$ is the birefringence of the liquid crystal at the crystalline state (or $T = 0$ K), the exponent $\beta = 0.2542$ is the material constant, $T_c = 330$ K is the clearing temperature, $A = 1.7230$ and $B = 5.24 \times 10^{-4}$ K^{-1} are the constants based on fitting of experimental measurements of the LC birefringence [46]. These dependencies are plotted in Figure S3 of the Supporting Information.

An application of a bias voltage across the LC cell results in rotation of the LC molecules and corre-

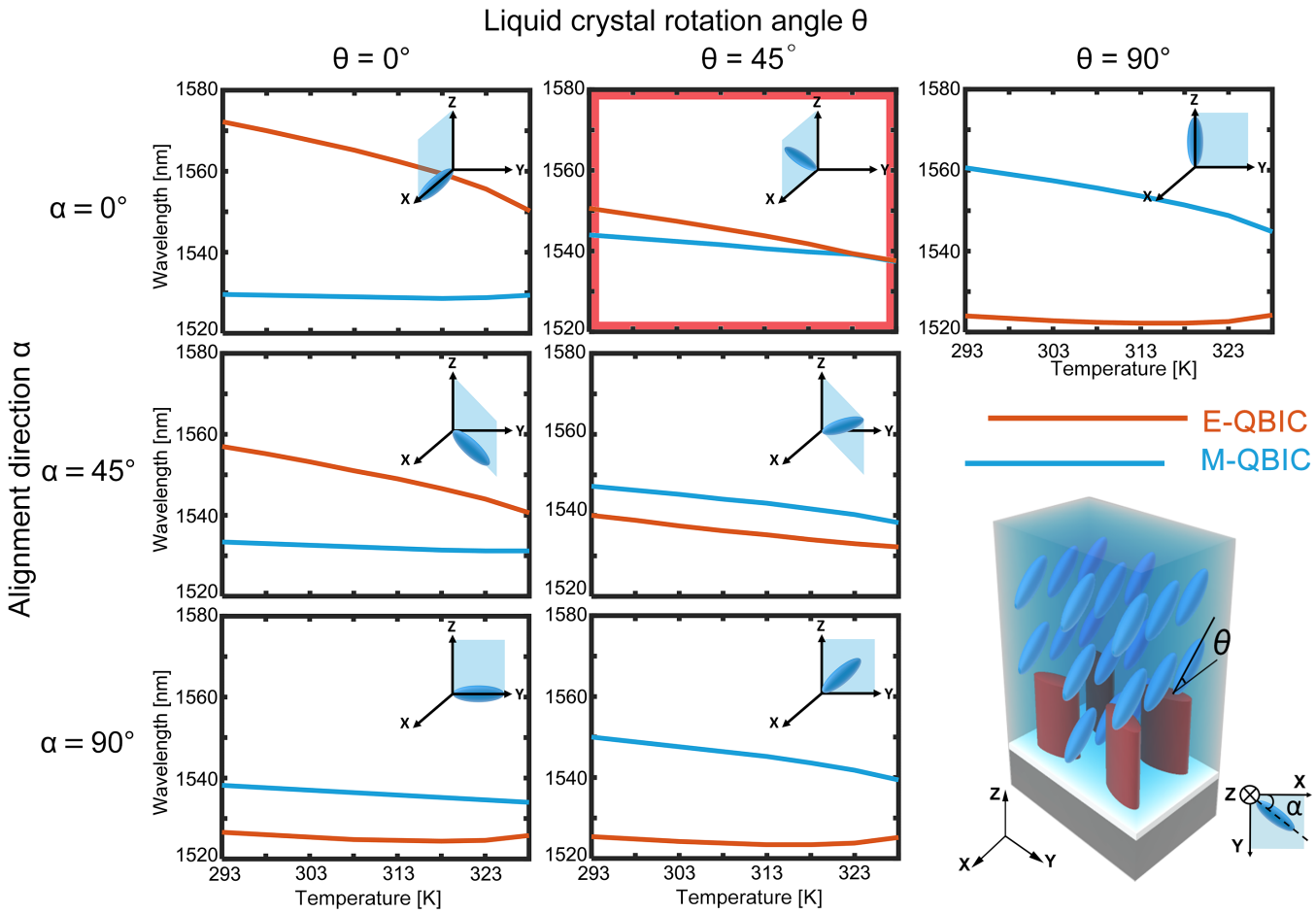

Figure 4: LC infiltrated metasurface tuning through change of voltage and temperature. Diagrams of the position of resonances through changes in the rotation angle of LC molecules (voltage tuning) and LC refractive index (temperature tuning). The insets in the upper right corner show the LC molecule spatial orientation. θ is the LC rotation angle between the LC molecule and $x - y$ plane and α is the alignment direction between the x-axis and the projection of the LC molecule in the $x-y$ plane. The design parameters of the unit-cell are $X = 900$ nm, $Y = 1331$ nm, $a = 240$ nm, $b = 80$ nm, $h = 520$ nm, and $\beta = 8°$.

spondingly to change of the effective refractive index. The effective refractive index can be described based on the general description of an anisotropic material after rotation of the crystalline axes by using Euler coordinate transformation,

$$\hat{n} = \hat{\rho}(\alpha, \theta, \psi) \begin{bmatrix} n_o & 0 & 0 \\ 0 & n_o & 0 \\ 0 & 0 & n_e \end{bmatrix} \hat{\rho}(\alpha, \theta, \psi)^{-1}. \tag{5}$$

Here, $\hat{\rho}$ is the rotation matrix, α denotes the rotation around the z-axis, θ is the angle between the new z axis and the $x - y$ plane, and the ψ is the rotation around the new z axis after the θ rotation, see the image in Figure 4.

Since the LC is a uniaxial material, we limit the description of the LC rotation to two angles, α and θ. As a starting point, we assume that the LC orientation is homogeneous in the volume of the LC cell, as shown in the image of Figure 4. The plots in Figure 4 show the calculated resonance positions of the E-QBIC (orange lines) and the M-QBIC (blue line) for different orientations of the LC molecules and different ambient temperatures. The angle α corresponds to the preset in-plane alignment direction, while the angle θ can be manipulated by the application of a bias voltage. As the temperature increases, the equivalent refractive index of the liquid crystal decreases, as described by Equation 1. As a result, there is an overall trend that the resonant frequencies of electric and magnetic Q-BICs shift to shorter wavelengths (Figure 4). When the LC molecules are aligned with the x-directions, ($\theta = 0°, \alpha = 0°$), the E-QBIC resonance position changes faster than the M-QBIC, when the LC molecules are aligned along the y-direction ($\theta = 0°, \alpha = 90°$), both resonances exhibit only weak tuning, when along the z-direction ($\theta = 90°$), the tuning of the M-QBIC resonances is faster than the one of the E-QBIC. These three cases therefore resemble the behavior of tuning of n_{xx}, n_{yy}, and n_{zz}, shown in Figure 2, respectively.

To achieve the same tuning rate for both resonances, it is necessary to adjust the effective indices for the x, y, and z electric field components. For this reason, we rotate the LC molecules in the $x - z$ plane. When $\alpha = 0°$ and $\theta = 45°$, as the temperature increases from 293 K (20°C) to 328 K (55°C), the electric resonance moves 13 nm and the magnetic resonance moves 6.4 nm, Figure 4. Continuously rotating the LC molecules (θ) or changing the alignment direction (α) can further optimize the tuning rates of the two resonances. However, there are some practical considerations that limit the available choice of tuning range. For example, when α is between 0° and 90°, the polarization state of the transmitted light will also be rotated, which is not desirable. In addition, excessive rotation of θ can cause a refractive index mismatch between the LC and the substrate, i.e. causing bianisotropy. With the high-Q resonances involved, such small refractive index mismatch can result in a bianisotropy-induced anti-crossing of the electric and magnetic QBICs, thereby destroying the Huygens condition. We found that the equivalent refractive index of the LC at $\theta = 45°$, as seen by the resonances, matches the refractive index of the substrate ($n = 1.6525$) without inducing anti-crossing. Considering these practical constrains, we use the configuration $\theta = 45°, \alpha = 0°$ (highlighted in Figure 4) as the basis for equalising the rates of the two resonances in a practically realisable situation for phase-only tuning.

To find the condition for pure phase SLM device, we utilise a bias voltage control of the LC rotation angle. We further take into account the spatial inhomogeneity of the LC orientation along the thickness of

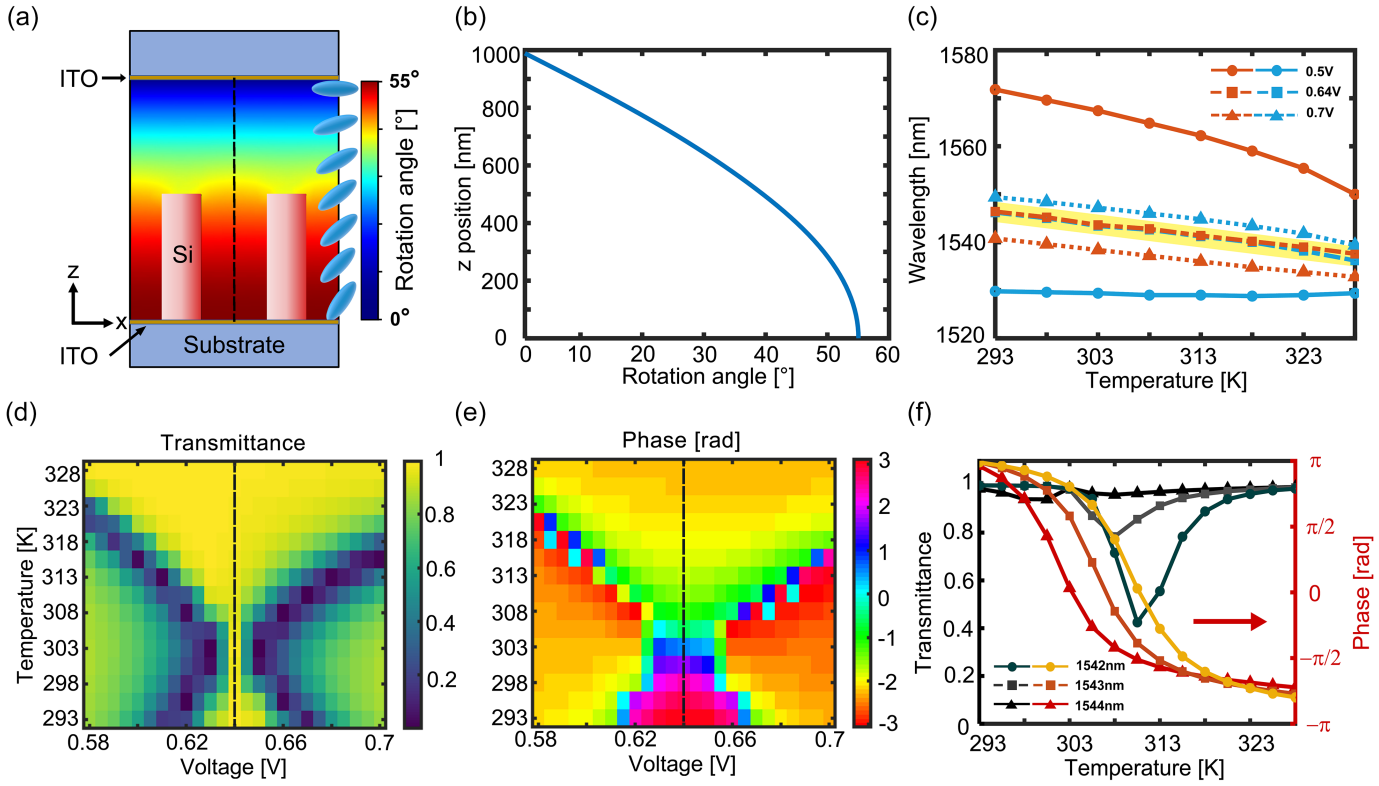

Figure 5: Pure phase tuning of extreme Huygens metasurfaces excited by an x-polarized plane wave. (a) Schematic view of LC angle distribution in the metasurface unit-cell. (b) The profile of LC molecules rotation angle along the black dash line in (a). (c) Tunability of the electric and magnetic resonances at 0.5 V, 0.64 V (yellow highlight) and 0.7 V. (d) Simulated transmittance and (e) phase as functions of voltage and temperature at 1544 nm near the Huygens regime. (f) Simulated transmittance and phase of at wavelengths of 1542 nm, 1543 nm and 1544 nm; the voltage is 0.64 V and the temperature varies from 293 K to 328 K.

the LC cell. The voltage controlled LC rotation angle can be expressed by the equation

$$K\nabla_z^2\theta + \frac{1}{2}\epsilon_0\Delta\epsilon\,|E_z(\mathbf{r})|^2\sin(2\theta) = 0, \tag{6}$$

where K is elastic constant of the LC. Because the dominant LC deformation due to the bias voltage is transverse strain (S-strain), for simplicity we use a single constant approximation, $K = K_{11} = K_{22} = K_{33} = 11.1$ pN. $\Delta\epsilon = 14.1$ is the dielectric constant anisotropy of LC at 1 kHz (control of the LC molecules orientation requires AC voltage in the kHz range to avoid charging). In order to simulate the real geometry of the LC cell, we also include an alignment layer on the top of the unit-cell, where the LC molecules are bound along the surface alignment direction. This phenomenon is known as surface anchoring that means the angle of the LC molecules is fixed to 0 degree at the boundary.

According to the above arrangements, we perform electromagnetic simulations of the transmission through the zig-zag metasurface integrated in a 1 μm thick LC cell. Figure 5a illustrates the LC molecules rotation angle distribution induced by the external bias voltage. The color bar represents the rotation an-

gle from zero (horizontal orientation) to 55° from the $x-y$ plane. The inhomogeneous LC distribution in the middle of the unit cell near the metasurface is due to the silicon elliptical cylinders influence the electric field. Without loss of generality, in our optical simulations, we have neglected the influence of the indium-tin-oxide (ITO) layer, which simply attenuates the overall transmission through the cell (see also section 5 of the Supporting Information). Figure 5b further depicts the LC rotation angle along the z-axis at the middle of the unit cell, marked with the black dash line in Figure 5a. This inhomogeneous LC distribution results in higher refractive index at the top of the unit cell, which also helps counteract the substrate induced bi-anisotropy, thereby allowing for a broader bandwidth of the Huygens condition.

Taking into account the LC inhomogeneous LC distribution induced by surface anchoring and the presence of the silicon elliptical pillars, we obtain the results for the metasurface transmission at different voltages and temperatures, shown in Figure 5c-f. Figure 5c shows the wavelength of the electric and magnetic resonance as a function of the temperature change at three different bias voltages. It can be seen that the two resonances will overlap together while satisfying the Huygens condition for a range of temperatures when the bias voltage is 0.64 V (highlighted in yellow). This complete Huygens regime is achieved for a wavelength around 1544 nm.

Figures 5d,e demonstrate the key result of our work. They show the simulated transmittance and phase profiles, at the wavelength of 1544 nm. It can be seen that an exact Huygens regime can be achieved with an applied bias voltage of 0.64 V, as a function of temperature, as marked with a black dash line in Figures 5d,e. We note that the advantage of our design is that it does not require the independent tuning of two control parameters, e.g. voltage and temperature. Instead, it provides a constant bias for the voltage, while still tuning a single control parameter only. As a result our geometry considerably simplifies the complexity of a possible pure-phase tuning SLM device.

Figure 5f gives an intuitive view of the achieved pure phase tuning with temperature, under the optimal bias-voltage for three different wavelengths (1542 nm, 1543 nm, and 1544 nm). Although all three wavelengths have achieved 2π phase tuning, the transmittance at 1544 nm shows higher efficiency than the others. The analysis of the bandwidth for the obtained pure phase tuning in this more realistic case shows that a tuning bandwidth of around 3.5 nm can be obtained (see also Figure S5 of the Supporting Information), which is suitable for operation with transform-limited pulses longer than 715 fs. While this bandwidth might not appear extraordinarily large, we would like to stress that it is twice larger than the FWHM of the individual resonances responsible for the extreme Huygens regime.

We believe that this bandwidth can be further increased by several optimisation strategies which can reduce the residual bi-anisotropy and/or increase the tunability of the resonances. For example, substrate over-etching or stronger vertical LC molecular inhomogeneity (rotation) could improve the bandwidth. In addition, the exploration of numerical free-form topology optimisation techniques could further open opportunities for increased bandwidth. However, these techniques remain outside of the scope of the current work, as the main focus of this work remains the general tuning concept and not the specific implementation.

3 Conclusions and discussion

In conclusion, we have provided a comprehensive study of the physical mechanisms of pure phase tuning of optical metasurfaces by optical anisotropy. In a nutshell, the optical anisotropy allows for the independent control of two parameters to only change the transmission phase while keeping the transmission efficiency at unity. Our results give new insights for achieving 2π-range pure phase tuning in transmissive optical metasurfaces, realised over a sizable bandwidth and with a small external stimulus. In particular, this pure phase tuning regime is achieved by exploring the effect of optical anisotropy on the QBIC of the metasurface.

Based on the obtain principles of anisotropic tuning, we have also proposed a practical realisation of our concept base on LC infiltrated metasurface operating in the extreme-Huygens regime. The potential of achieving a 2π pure-phase tuning is demonstrated numerically by controlling the molecular orientation of the surrounding LC, using a hybrid application of the bias voltage and the temperature. The phase only tuning is demonstrated over a bandwidth of 3.5 nm, which is about two times the full-width at half maximum bandwidth of the individual resonances and suitable for short pulse operation in telecommunication applications.

Importantly, the revealed concept and physical mechanism are general and not limited to the specific design or tuning mechanism shown. We would like to stress that other implementations could also be realised, including LC anisotropy control by vectorial electric field. For example, a three-dimensional (3D) control of the applied vecotorial bias field could also be employed for pure-phase tuning. Such vectorial bias vield would allow for a full rotation of the LC refractive index tensor therefore controlling the material anisotropy as required for pure phase tuning. Indeed, such 3D rotation could be realised by a

combination of LC in-plane switching and vertical alignment, which are well-established technologies in the LC industry. However, we believe that our choice of constant bias voltage and temperature tuning is more elegant tuning technique due to the single tuning parameter. Overall our work provides a new angle for further experimental studies and could benefit the development of more sophisticated functionalities such as dynamic beam-steering and dynamic holographic displays.

Conflict of Interest

The authors declare no conflict of interest.

Acknowledgements We acknowledge support by the Australian Research Council through the Centres of Excellence scheme (CE200100010). We thank I. Shadrivov and Y. Izdebskaya for the fruitful discussions.

References

[1] U. Efron, *Spatial light modulator technology: materials, devices, and applications*, volume 47, CRC press, **1994**.

[2] D. Neshev, I. Aharonovich, *Light: Science & Applications* **2018**, *7*, 1 1.

[3] A. I. Kuznetsov, A. E. Miroshnichenko, M. L. Brongersma, Y. S. Kivshar, B. Luk'yanchuk, *Science* **2016**, *354*, 6314 846.

[4] M. Decker, I. Staude, M. Falkner, J. Dominguez, D. N. Neshev, I. Brener, T. Pertsch, Y. S. Kivshar, *Adv. Opt. Mater.* **2015**, *3*, 6 813.

[5] A. Arbabi, Y. Horie, M. Bagheri, A. Faraon, *Nat. Nanotech.* **2015**, *10*, 11 937.

[6] M. Khorasaninejad, W. T. Chen, R. C. Devlin, J. Oh, A. Y. Zhu, F. Capasso, *Science* **2016**, *352*, 6290 1190.

[7] D. Lin, P. Fan, E. Hasman, M. L. Brongersma, *Science* **2014**, *345*, 6194 298.

[8] A. M. Shaltout, V. M. Shalaev, M. L. Brongersma, *Science* **2019**, *364*, 6441.

[9] C. Zou, I. Staude, D. N. Neshev, In *Dielectric Metamaterials*, 195–222. Elsevier, **2020**.

[10] S. Saha, D. Shah, V. M. Shalaev, A. Boltasseva, *Optics and Photonics News* **2021**, *32*, 7 34.

[11] M. M. Salary, H. Mosallaei, *ACS Photonics* **2020**, *7*, 7 1813.

[12] Y.-W. Huang, H. W. H. Lee, R. Sokhoyan, R. A. Pala, K. Thyagarajan, S. Han, D. P. Tsai, H. A. Atwater, *Nano letters* **2016**, *16*, 9 5319.

[13] M. C. Sherrott, P. W. Hon, K. T. Fountaine, J. C. Garcia, S. M. Ponti, V. W. Brar, L. A. Sweatlock, H. A. Atwater, *Nano letters* **2017**, *17*, 5 3027.

[14] G. K. Shirmanesh, R. Sokhoyan, P. C. Wu, H. A. Atwater, *ACS nano* **2020**, *14*, 6 6912.

[15] M. Rahmani, L. Xu, A. E. Miroshnichenko, A. Komar, R. Camacho-Morales, H. Chen, Y. Zárate, S. Kruk, G. Zhang, D. N. Neshev, et al., *Advanced Functional Materials* **2017**, *27*, 31 1700580.

[16] K. Zangeneh Kamali, L. Xu, J. Ward, K. Wang, G. Li, A. E. Miroshnichenko, D. Neshev, M. Rahmani, *Small* **2019**, *15*, 15 1805142.

[17] J.-Y. Ou, E. Plum, L. Jiang, N. I. Zheludev, *Nano letters* **2011**, *11*, 5 2142.

[18] A. L. Holsteen, S. Raza, P. Fan, P. G. Kik, M. L. Brongersma, *Science* **2017**, *358*, 6369 1407.

[19] E. Arbabi, A. Arbabi, S. M. Kamali, Y. Horie, M. Faraji-Dana, A. Faraon, *Nature communications* **2018**, *9*, 1 1.

[20] J. Sautter, I. Staude, M. Decker, E. Rusak, D. N. Neshev, I. Brenner, Y. S. Kivshar, *ACS Nano* **2015**, *9* 4308.

[21] A. Komar, Z. Fang, J. Bohn, J. Sautter, M. Decker, A. Miroshnichenko, T. Pertsch, I. Brener, Y. S. Kivshar, I. Staude, D. N. Neshev, *Appl. Phys. Lett.* **2017**, *110*, 7 071109.

[22] S.-Q. Li, X. Xu, R. Maruthiyodan Veetil, V. Valuckas, R. Paniagua-Domínguez, A. I. Kuznetsov, *Science* **2019**, *364*, 6445 1087.

[23] Y. Hu, X. Ou, T. Zeng, J. Lai, J. Zhang, X. Li, X. Luo, L. Li, F. Fan, H. Duan, *Nano Letters* **2021**.

[24] J. Li, P. Yu, S. Zhang, N. Liu, *Nature communications* **2020**, *11*, 1 1.

[25] P. Yu, J. Li, N. Liu, *Nano Letters* **2021**, *21*, 15 6690.

[26] A. Lininger, A. Y. Zhu, J.-S. Park, G. Palermo, S. Chatterjee, J. Boyd, F. Capasso, G. Strangi, *Proceedings of the National Academy of Sciences* **2020**, *117*, 34 20390.

[27] M. Bosch, M. R. Shcherbakov, K. Won, H.-S. Lee, Y. Kim, G. Shvets, *Nano Letters* **2021**, *21*, 9 3849.

[28] J. A. Dolan, H. Cai, L. Delalande, X. Li, A. B. Martinson, J. J. De Pablo, D. López, P. F. Nealey, *ACS Photonics* **2021**, *8*, 2 567.

[29] A. A. Komar, D. N. Neshev, A. E. Miroshnichenko, *JETP Letters* **2017**, *106*, 11 709.

[30] M. Parry, A. Komar, B. Hopkins, S. Campione, S. Liu, A. E. Miroshnichenko, J. Nogan, M. B. Sinclair, I. Brener, D. N. Neshev, *Applied Physics Letters* **2017**, *111*, 5 053102.

[31] A. Komar, R. Paniagua-Domínguez, A. Miroshnichenko, Y. F. Yu, Y. S. Kivshar, A. I. Kuznetsov, D. Neshev, *ACS Photonics* **2018**, *5*, 5 1742.

[32] C. Zou, A. Komar, S. Fasold, J. Bohn, A. A. Muravsky, A. A. Murauski, T. Pertsch, D. N. Neshev, I. Staude, *ACS Photonics* **2019**, *6*, 6 1533.

[33] J. Li, P. Yu, S. Zhang, N. Liu, *Nature Communications* **2020**, *11*, 1 3574.

[34] M. Liu, D.-Y. Choi, *Nano letters* **2018**, *18*, 12 8062.

[35] M. Liu, D. A. Powell, R. Guo, I. V. Shadrivov, Y. S. Kivshar, *Advanced Optical Materials* **2017**, *5*, 16 1600760.

[36] A. Tittl, A. Leitis, M. Liu, F. Yesilkoy, D.-Y. Choi, D. N. Neshev, Y. S. Kivshar, H. Altug, *Science* **2018**, *360*, 6393 1105.

[37] C. W. Hsu, B. Zhen, A. D. Stone, J. D. Joannopoulos, M. Soljačić, *Nature Reviews Materials* **2016**, *1*, 9 1.

[38] K. Koshelev, S. Lepeshov, M. Liu, A. Bogdanov, Y. Kivshar, *Physical review letters* **2018**, *121*, 19 193903.

[39] J. Tian, Q. Li, P. A. Belov, R. K. Sinha, W. Qian, M. Qiu, *ACS Photonics* **2020**, *7*, 6 1436.

[40] D. A. Powell, Y. S. Kivshar, *Applied Physics Letters* **2010**, *97*, 9 091106.

[41] T. Weiss, M. Schäferling, H. Giessen, N. Gippius, S. Tikhodeev, W. Langbein, E. Muljarov, *Physical Review B* **2017**, *96*, 4 045129.

[42] A. Minovich, D. N. Neshev, A. Dreischuh, W. Krolikowski, Y. S. Kivshar, *Opt. Lett.* **2007**, *32*, 12 1599.

[43] Q. Yang, S. Kruk, Y. Xu, Q. Wang, Y. K. Srivastava, K. Koshelev, I. Kravchenko, R. Singh, J. Han, Y. Kivshar, et al., *Advanced Functional Materials* **2020**, *30*, 4 1906851.

[44] P.-G. De Gennes, J. Prost, *The physics of liquid crystals*, 83. Oxford university press, **1993**.

[45] I.-C. Khoo, *Liquid crystals*, volume 64, John Wiley & Sons, **2007**.

[46] J. Li, S.-T. Wu, S. Brugioni, R. Meucci, S. Faetti, *Journal of Applied Physics* **2005**, *97*, 7 073501.

[47] C. Zou, C. Amaya, S. Fasold, A. A. Muravsky, A. A. Murauski, T. Pertsch, I. Staude, *ACS Photonics* **2021**.